Catalysis Communications 69 (2015) 212–216

Contents lists available at ScienceDirect

Catalysis Communications

journal homepage: www.elsevier.com/locate/catcom

Short communication

CO oxidation over Au supported on Mn–ZSM5 and Mn–MOR

Juan M. Zamaro [a], Alicia V. Boix [a], Angel Martínez-Hernández [b,*]

[a] Instituto de Investigaciones en Catálisis y Petroquímica, INCAPE (FIQ, UNL, CONICET), Santiago del Estero 2829, C.P. 3000 Santa Fe, Argentina
[b] Universidad Autónoma de Nuevo León, UANL, Facultad de Ciencias Químicas, Av. Universidad S/N, San Nicolás de los Garza, Ciudad Universitaria, C.P. 66451 N.L., Mexico

ARTICLE INFO

Article history:
Received 30 April 2015
Received in revised form 20 June 2015
Accepted 23 June 2015
Available online 28 June 2015

Keywords:
Gold
Manganese
Zeolite
Catalysts
CO oxidation

ABSTRACT

Active gold catalysts for CO oxidation were obtained by the deposition–precipitation of gold on ZSM-5 and mordenite, both of them ion-exchanged with manganese. A strong promotion of Mn upon the activity of bimetallic Au/Mn catalysts was observed when compared with the monometallic Au–zeolites. In turn, when an in-situ reduction of the bimetallic catalysts was performed, a further increase in activity was observed. Characterizations suggested that smaller gold nanoparticles were stabilized in the bimetallic solids and that the reduction process caused a rearrangement of Au and Mn species on the catalyst surface.

1. Introduction

The catalytic oxidation of carbon monoxide is a reaction of environmental significance [1,2]. Among the numerous catalyst formulations that have been investigated, those based on gold particles of nanometer size have received increasing attention due to their good catalytic activity at low temperatures. Since the pioneering work of Haruta et al. [3], catalyst formulations have improved. Gold catalysts supported on reducible metal oxides such as TiO_2, CeO_2 and ZrO_2 have been proposed [4,5] since one of the decisive steps in the reaction mechanism occurs at the support-metal interface on Au–O sites. Moreover, it has been reported that the activity of gold-based catalysts can be improved by the addition of Mn and Fe oxides [6]. On the other hand, the use of zeolites can improve the dispersion of small metal clusters due to their controlled pore size and topology [7]. In this line, several Au–zeolites catalysts have been employed for the oxidation of CO; in most of these studies, gold species were incorporated by ion-exchange followed by calcination treatments where the segregation of gold as metallic Au nanoparticles ensued [8–11]. Considering that MOR and ZSM5 allow a high dispersion of Mn^{+2} via the ion-exchange process and that they have high specific surface area, the idea of achieving a high dispersion of gold nanoparticles with a close Au–Mn interaction seems reasonable. In this context, the aim of this work is to study the catalytic activity of gold nanoparticles introduced by deposition–precipitation on Mn-exchanged zeolites for the CO oxidation reaction.

2. Experimental

2.1. Catalyst preparation and catalytic evaluation

NH_4–ZSM5 (Zeolyst, $SiO_2/Al_2O_3 = 30$) and NH_4–mordenite (Zeolyst, $SiO_2/Al_2O_3 = 20$) were used. These supports were firstly ion-exchanged with a Na^+ solution (sodium acetate, Aldrich) and then were again ion-exchanged with a solution of $Mn(NO_3)_2 \cdot 4H_2O$ (Aldrich); (3 g zeolite, 250 ml solution 1×10^{-3} M, three times at r.t.). The solids were filtered, washed and dried. Then, Au was deposited on Mn–zeolite solids by the deposition–precipitation method [12]. Briefly, this consisted in slowly adding a solution of $HAuCl_4 \cdot 3H_2O$ (Fisher 99%) to the support suspended in water, keeping the pH fixed at 9. Finally, the solids were filtered, washed and calcined (500 °C, 4 h) and were labeled as Au(x)/Mn–MOR and Au(x)/Mn–ZSM5, respectively, where x indicates the % w/w of gold as determined by Atomic Absorption Spectroscopy (Table S1). Monometallic Au–zeolite samples were also prepared. Some samples were submitted to in-situ oxidation (air, 400 °C, 30 min) or reduction ($H_2 - N_2$, 300 °C, 60 min) pretreatments. The CO oxidation reaction was carried out in a tubular quartz reactor using 300 mg of catalyst and a reaction mixture flow of 100 cm^3 min^{-1} with a composition of 2% (v/v) CO and 2% O_2 (v/v) in N_2 balance. The reactants and products were analyzed on line by GC (HP 5890 series II).

2.2. Catalyst characterization

The elemental content of Au, Mn and Na was determined by Atomic Absorption Spectroscopy (Varian SpectrAA 220FS). X-ray Diffraction was performed on a Siemens D-5000 diffractometer (Cuk_α radiation, $\lambda = 1.5406$ Å). Transmission Electron Microscopy analyses were

* Corresponding author at: Universidad Autónoma de Nuevo León, Facultad de Ciencias Químicas, Av. Universidad S/N, San Nicolás de los Garza, Ciudad Universitaria, C.P. 66451 N.L., Mexico.
E-mail address: angel.martinezhn@uanl.edu.mx (A. Martínez-Hernández).

http://dx.doi.org/10.1016/j.catcom.2015.06.018
1566-7367/

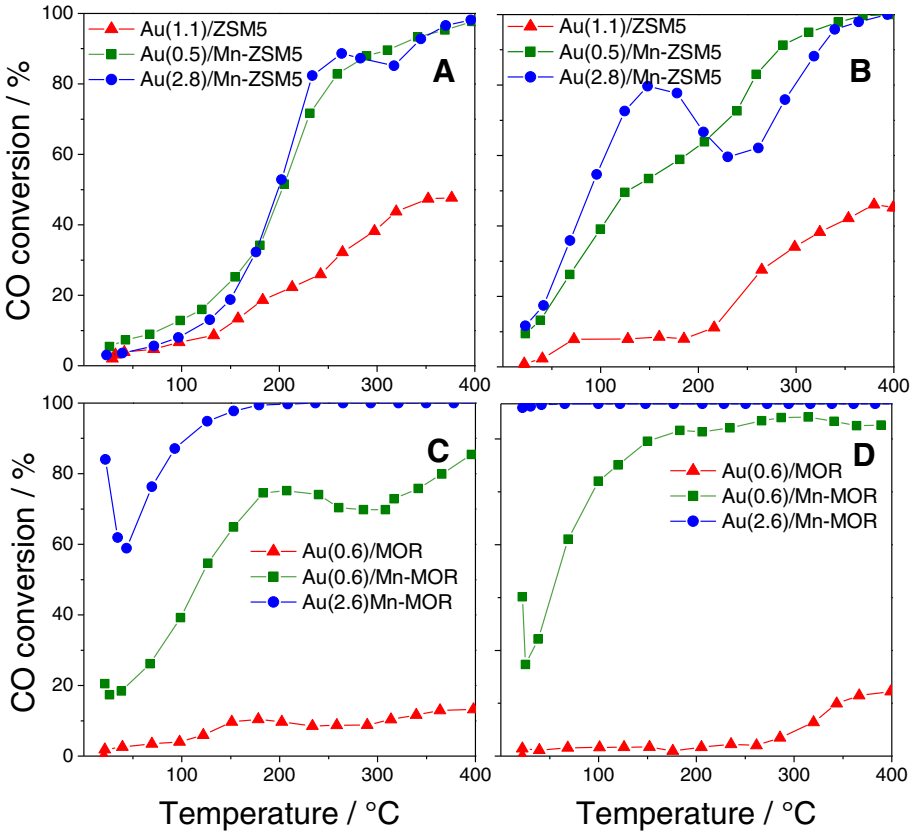

Fig. 1. CO conversion curves. Au/ZSM5 and Au(x)/Mn–ZSM5: A) calcined; B) reduced. Au/MOR and Au(x)/Mn–MOR: C) calcined; D) reduced.

performed in a JEOL 2000 FXII instrument. UV–vis spectroscopy (Varian Cary 5E) was performed using a diffuse reflectance accessory in a controlled atmosphere chamber. The CO-FTIR spectra were obtained using a Shimadzu FTIR 8101M spectrometer. The samples were outgassed and then reduced in-situ or oxidized. Different CO pressures (1.3×10^3 Pa, 6.6×10^3 Pa, 1.3×10^4 Pa) were admitted and then evacuated for 30 min at room temperature, 50 °C and 100 °C, and the spectrum was taken (details in SI). XPS analyses (SPECS) were performed (pass energy 30 eV; Al Kα X-ray source, 200 W, 12 kV). Spectra were acquired in the Au 4f, Au 4d, Mn 2p, Al 2p, Si 2p, and C 1s regions. The binding energy of Si 2p peak was taken as reference, 103.2 eV or 102.8 eV for ZSM5 or MOR catalysts, respectively. The data processing was performed using the Casa XPS software.

3. Results and discussion

3.1. Metal loading and catalytic activity

When gold was deposited in Na–MOR and Na–ZSM-5, 0.6 wt.% and 1.1 wt.% of Au were obtained, respectively (Au(0.6)/MOR and Au(1.1)/ZSM5). However, for Mn–zeolites the amount of Au deposited was higher (Au(2.6)/Mn–MOR and Au(2.8)/Mn–ZSM5). Since the conditions were the same in all preparations, the difference may be due to a higher affinity of gold to be deposited on manganese [13]. Bimetallic solids with a lower amount of gold (Au(0.6)/Mn–MOR and Au(0.5)/Mn–ZSM5), were also obtained. On the other hand, the amount of exchanged Mn was constant for each zeolite, around 0.9 wt.% for

Table 1
XPS results of Au supported on Mn–ZSM5 and Mn–MOR.

Catalyst	Binding energies and fwhm (eV)				Surface atomic ratio	
	Au $4f_{5/2}$	Au $4f_{7/2}$	Mn $2p_{1/2}$	Mn $2p_{3/2}$	Au/Al	Mn/Al
Au(1.1)/ZSM5	87.2 (1.9)	83.6 (1.9)	–	–	0.58	–
Reduced[a]	87.3 (1.9)	83.8 (1.9)	–	–	0.56	–
Au(0.6)/MOR	86.6 (2.2)	83.1 (2.2)	–	–	0.03	–
Reduced[a]	86.8 (1.9)	83.3 (1.9)	–	–	0.01	–
Au(2.8)/Mn–ZSM5	87.2 (2.1)	83.6 (2.1)	654.4 (5.1)	642.2 (5.1)	0.06	0.30
Reduced[a]	87.3 (1.9)	83.7 (1.9)	655.3 (4.6)	642.8 (4.6)	0.08	0.31
Au(2.6)/Mn–MOR	86.3 (2.2)	82.5 (2.2)	651.5 (4.4)	640.0 (4.4)	0.04	0.31
Reduced[a]	86.7 (2.0)	83.2 (2.0)	652.4 (5.1)	641.2 (5.1)	0.03	0.36
After reaction[c]	86.3 (1.9)	82.4 (1.9)	651.7 (4.0)	639.9 (4.0)	0.03	0.33
Mn–ZSM5	–	–	654.6 (4.0)	642.5 (4.0)	–	0.24
Mn–MOR	–	–	654.6 (3.2)[b] 659.8 (5.5)	642.5 (3.2) 645.0 (5.5)	–	0.28

[a] Samples reduced in-situ.
[b] The concentration of this component was 66%.
[c] Sample analyzed after their catalytic evaluation.

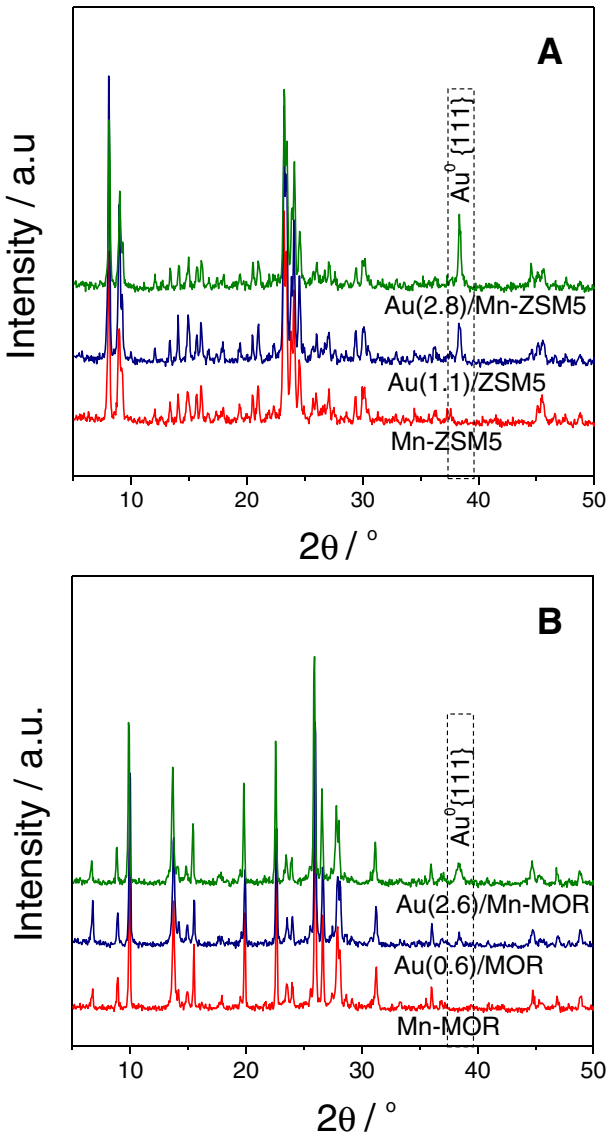

Fig. 2. XRD patterns: A) Au(1.1)/ZSM5 and Au(2.8)/Mn–ZSM5; B) Au(0.6)/MOR and Au(2.6)/Mn–MOR.

ZSM5 and 2.0 wt.% for MOR, respectively (Table S1). The higher manganese content on MOR is because it has a lower SiO_2/Al_2O_3 ratio. After the ion-exchange with manganese solution the Na content was 1.7 wt.% for Mn–ZSM5 and 2.0 wt.% for Mn–MOR, which did not change with the Au deposition.

It can be seen that calcined Au(1.1)/ZSM5 (Fig. 1A) presented moderate activity (conversion < 50% at 400 °C). However, when Au sites were modified by Mn species, the conversion increased in all temperature ranges. When the in-situ reduction treatment was carried out (Fig. 1B), a remarkable shift of the activity to low temperature in the bimetallic samples was observed, whereas the activity remained almost unchanged for the monometallic catalyst. An inflection in the conversion curves became more pronounced in the sample with higher Au loading (Fig. 1B). This is associated with the presence of a dual system of sites, with optimal catalytic activity at different temperature ranges, as it has been suggested for other Au–zeolite catalysts [8].

Similarly, the activity of calcined Au(0.6)/MOR (Fig. 1C) was low; in addition, it was inferior to those observed for Au(1.1)/ZSM5 which was expected due to the lower Au content. Furthermore, an increase of activity on bimetallic solids was noted which clearly shows a promoting effect of Mn. A similar behavior was reported for catalysts of gold supported on Fe–zeolites [14]. The highly active Au(2.6)/Mn–MOR sample showed a slight deactivation with the time on stream in catalytic tests at different temperatures (Fig. S1). This sample after reaction exhibited BEs of Au and Mn similar to those of the oxidized sample (Table 1).

Considering that the Mn–MOR and Mn–ZSM5 solids presented very low activity at low temperatures (Fig. S2), the promoting effect could be attributed to a greater stabilization of small Au clusters, which are the most active species for the oxidation of CO at low temperatures [15]. Furthermore, the in-situ reduction of Au/Mn–MOR samples caused a notable increase in the activity, but there was no change in the monometallic samples (Fig. 1D).

3.2. Catalyst structure

After the exchange with Mn and Au deposition, both zeolites retain their framework integrity (Fig. 2). For all catalysts, the main signal of metallic gold at $2\theta = 38.5°$ (plane {111}) was observed. In agreement with the highest Au loading, this peak becomes more intense for the Mn-exchanged samples. The mean crystallite size of Au^0 (details in SI) for Au(0.6)/MOR was 34 nm, while for Au(2.6)/Mn–MOR it decreased to 17 nm. In the case of Au–ZSM5, the size of Au^0 particles was 30 nm with or without the presence of Mn. There were no relevant structural

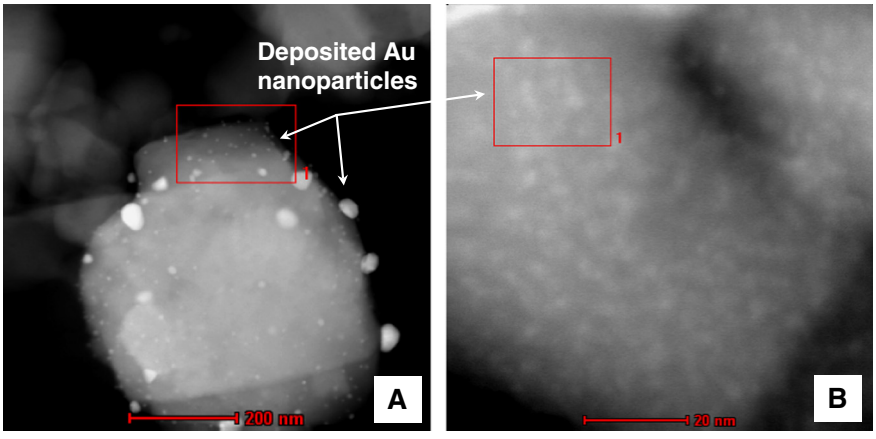

Fig. 3. TEM images of: A) Au(0.6)MOR; B) Au(2.6)/Mn–MOR.

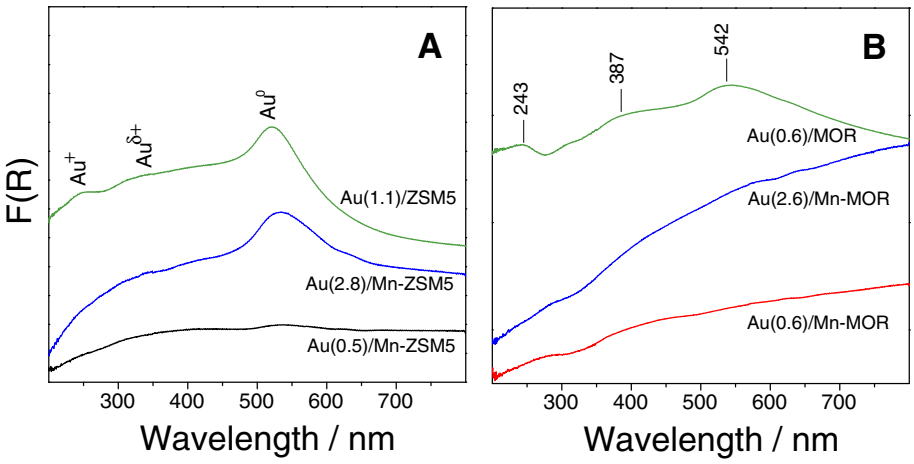

Fig. 4. UV–vis spectra: A) ZSM-5 catalysts; B) Mordenite catalysts.

changes for the bimetallic samples after oxidation or reduction treatments (Fig. S3). Heterogeneity in the gold particles sizes was observed by TEM, with a large dispersion of sizes for Au(0.6)/MOR ranging from 7–50 nm (Fig. 3A), whereas for Au(2.6)/Mn–MOR the size distribution was somewhat narrower (2–15 nm). In the case of the latter sample, a larger fraction of the nanoparticles observed had a size of less than 10 nm (Fig. 3B). In the case of ZSM5 catalysts, the situation was similar, with Au(1.1)/ZSM5 having a wide dispersion (10–100 nm), whereas was some narrower in Au(2.8)/Mn–ZSM5 (40–90 nm).

3.3. Spectroscopic characterizations

In the UV–vis spectra of ZSM5 catalysts (Fig. 4A) the presence of gold nanoparticles (Au^0), partially charged gold clusters ($Au^{\delta+}$) and cationic gold species (Au^+ or Au^{3+}) can be observed [8,16]. In the Au–MOR catalysts (Fig. 4B), the above bands were weaker but in spite of that, the three types of gold clusters can be distinguished. In the monometallic catalyst, the most intense bands suggest that the formation of "larger" metallic gold nanoparticles is favored. However, in Au/Mn–MOR solids the weak intensity of the bands indicates gold nanoparticles of very small size. The decrease of the intensity in the UV bands (particularly the plasmon resonance) with the size of the gold particle was shown by Tuzovskaya et al. [16].

The CO-FTIR spectra (Fig. 5) show a complex band due to the stretching of CO adsorbed on the different metals (Au, Mn, Na). Additionally, CO can be adsorbed in unsaturated Al^{3+} sites of the zeolite [17]. For all the samples studied, despite the pretreatment, the position of the bands does not change with respect to that of the evacuated samples. This could indicate that the electronic modifications of the gold species by the pretreatments are very small. Au(1.1)/ZSM5 (Fig. 5A) shows the stretching of CO adsorbed on Au^0 (2112 cm^{-1}) and of CO–Na^+ (2174 cm^{-1}), although it may also be superimposed onto CO–Au^+. The weak signals at 1982 and 2050 cm^{-1} are associated with CO–$Au^{\delta-}$ [9]. In Au(2.8)/Mn–ZSM5, the band of CO–Na^+ decreases due to the ion-exchange whereas an intense band at 2212 cm^{-1} develops due to manganese carbonyl species [18]. For this catalyst, weak bands attributed to the adsorption of CO on $Au^{\delta-}$ and Au^0 sites were also identified. Au(0.6)/MOR (Fig. 5B) showed bands of CO–Na^+ (2176 cm^{-1}) and CO–Au^{δ} (1983 and 2026 cm^{-1}) whereas for Au(2.6)/Mn–MOR, an intense band due to CO–Mn^{2+} was developed (2198 cm^{-1}) and that of CO–Na^+ decreased. Additionally, for all these solids, the presence of a composed band around 2356 cm^{-1} was present (Fig. 5), which is attributed to CO_2 adsorbed linearly to cations. Since in our samples the main species are exchanged Mn^{+2} and deposited Au^0, CO_2 is most probably associated with a CO disproportionation during adsorption at exchange sites (acid Lewis sites) [17] and suggests a possible carbonate formation on the surface during reaction [12].

The XPS results are summarized in Table 1. The Au 4f and Mn 2p spectral regions of bimetallic catalysts were analyzed considering the overlapping of spectra, namely, the contribution of the Mn 3s signal (c.a. 83 eV) in the Au 4f spectral region and also the contribution of the Au $4p_{1/2}$ peak in the Mn 2p region. The Au $4f_{7/2}$ binding energies (BE) for Au(1.1)ZSM5 and Au(2.8)/Mn–ZSM5 at 83.6 eV are typical of metallic Au [19]. After in situ reduction, these values were unchanged.

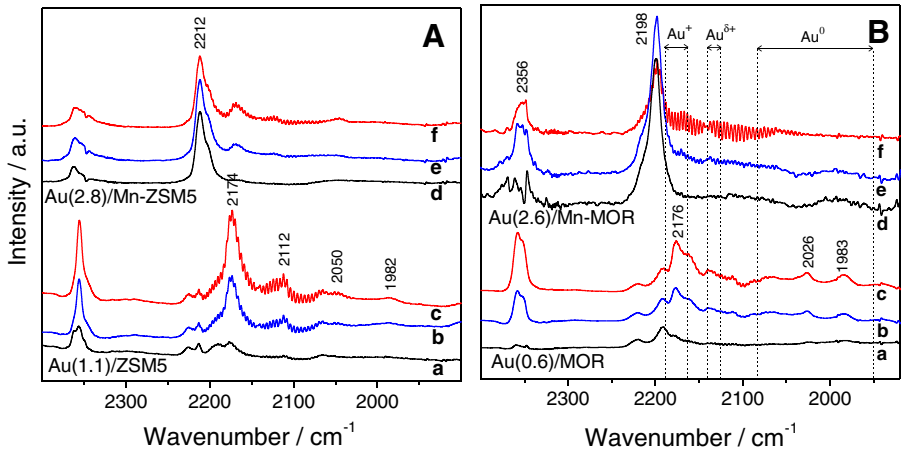

Fig. 5. CO-FTIR after in-situ reduction: A) Au(1.1)/ZSM5 and Au(2.8)/Mn–ZSM5; B) Au(0.6)/MOR and Au(2.6)/Mn–MOR. (a, d: 1.3×10^3 Pa; b, e: 6.6×10^3 Pa; c, f: 1.3×10^4 Pa).

Similarly, the BE measured on Au(0.6)/MOR and Au(2.6)/Mn–MOR were 83.1 and 82.5 eV, respectively. When the catalysts were reduced in situ, Au 4f BEs showed no significant changes, except for Au(2.6)/Mn–MOR. In the reduced Au(1.1)ZSM5 and Au(0.6)/MOR, the BE values increased 0.2 eV, which could be associated with a slight variation in the particle sizes of gold due to the reduction process. The surface molar ratio (Au/Al) was about 0.58–0.56 in Au(1.1)ZSM5, but lower for Au(0.6)/MOR, according to the Au loading. The most notable shift of BE was observed for Au(2.6)/Mn–MOR after the reduction treatment which can be related to the small size of gold nanoparticles as observed with the other characterization techniques.

The BEs of the Mn $2p_{1/2}$–Mn $2p_{3/2}$ region on Au(2.8)/Mn–ZSM5 can be associated with Mn^{2+} and Mn^{3+} species [20] because of the broadening of the peaks different from Mn/ZSM5 where the width is narrower. Moreover, a higher Mn/Au surface ratio after the reduction process (Table 1) was observed on Au(2.6)/Mn–MOR compared to Au(2.8)/Mn–ZSM5 (12 and 3.9, respectively). The smaller Au particle size and the higher Mn/Au ratio in the surface of the Au(2.6)/Mn–MOR may be the reason for the stronger interaction between Au–Mn species, which improves the catalytic activity of this solid.

4. Conclusions

Catalysts based on gold nanoparticles obtained by deposition–precipitation on Mn-exchanged mordenite and ZSM5 showed high activity towards CO oxidation. The effect of Mn appears to be related to the stabilization of small gold nanoparticles deposited on these solids, which are the most active species at low temperatures. Moreover, a reduction treatment induces a rearrangement of the species that in Au/Mn–mordenite increases the surface Mn/Au ratio, thereby improving the interaction between Au and Mn, having as a result an increase in the catalytic activity of this solid.

Acknowledgments

The authors wish to acknowledge the financial support received from CONICET, ANPCyT (PICT 1299), Universidad Nacional del Litoral (CAI+D 0486) and Universidad Autónoma de Nuevo León (PAICYT: IT148-9 and IT-641-11). Thanks are also given to ANPCyT for the purchase of the UHV Multi Analysis System (PME 8-2003) and to Fernanda Mori for the XPS analyses.

Appendix A. Supplementary data

Experimental procedures for estimation of crystallite size by X-ray diffraction, CO-FTIR spectroscopy and long term catalytic tests. Metal loading (by AAS) in zeolites, time on-stream studies, catalytic activity of Mn–zeolites and XRD of Au/Mn–zeolites treated by oxidation or reduction. Supporting information (SI) for this article can be found online at http://dx.doi.org/10.1016/j.catcom.2015.06.018.

References

[1] E. Green, S. Short, IEH Assessment on Indoor Air Quality in the Home (2): Carbon Monoxide, 1998. (Leicester).
[2] H. Igarashi, T. Fujino, M. Watanabe, J. Electroanal. Chem. 391 (1995) 119–123.
[3] M. Haruta, T. Kobayashi, H. Sano, N. Yamada, Chem. Lett. (1987) 405.
[4] L. Chang, Y. Yeh, Y. Chen, Int. J. Hydrog. Energy 33 (2008) 1965–1974.
[5] I. Dobrosz-Gómez, I. Kocemba, J. Rynkowski, Appl. Catal., B 83 (2008) 240–255.
[6] J. Margitfalvi, M. Hegedús, Á. Szegedi, I. Sajó, Appl. Catal., A 272 (2004) 87–97.
[7] Zeolites and ordered mesoporous materials: Progress and prospects, Stud. Surf. Sci. Catal. 157 (2005) 337–366.
[8] A. Simakov, I. Tuzovskaya, A. Pestryakov, N. Bogdanchikova, V. Gurin, M. Avalos, M. Farías, Appl. Catal., A 331 (2007) 121–128.
[9] I. Tuzovskaya, A. Simakov, A. Pestryakov, N. Bogdanchikova, V. Gurin, M. Farías, H. Tiznado, M. Avalos, Catal. Commun. 8 (2007) 980–997.
[10] J. Chen, J. Lin, Y. Kang, W. Yu, C. Kuo, B. Wan, Appl. Catal., A 291 (2005) 162–169.
[11] J. Fierro-Gonzalez, B. Gates, J. Phys. Chem. B 108 (44) (2004) 16999–17002.
[12] R. Ramírez-Garza, B. Pawelec, T. Zepeda, A. Martínez-Hernández, Catal. Today 172 (2011) 95–102.
[13] S. Gardner, G. Hoflund, M. Davidson, Langmuir 7 (1991) 2140–2145.
[14] N. Bogdanchikova, A. Simakov, E. Smolentseva, A. Pestryakov, M. Farias, J. Diaz, A. Tompos, M. Avalos, Appl. Surf. Sci. 254 (2008) 4075–4083.
[15] M. Haruta, Catal. Surv. Jpn. 1 (1997) 61–73.
[16] I. Tuzovskaya, N. Bogdanchikova, A. Simakov, V. Gurin, A. Pestryakov, M. Avalos, M. Farías, Chem. Phys. 338 (2007) 23–32.
[17] V. Rakic, R. Hercigonja, V. Dondur, Microporous Mesoporous Mater. 27 (1999) 27–39.
[18] M. Campa, D. Pietrogiacomi, S. Tuti, G. Ferraris, V. Indovina, Appl. Catal., B 18 (1998) 151–162.
[19] T. Zepeda, A. Martinez-Hernández, R. Guil-López, B. Pawelec, Appl. Catal., B 100 (2010) 450–462.
[20] M. Biesinger, B. Payne, A. Grosvenor, L. Lau, A. Gerson, R. Smart, Appl. Surf. Sci. 257 (2011) 2717–2730.